New Methods of Particle Collimation in Colliders

Giulio Stancari*
Fermi National Accelerator Laboratory, P.O. Box 500, Batavia, Illinois 60510, USA

The collimation system is an essential part of the design of any high-power accelerator. Its functions include protection of components from accidental and intentional energy deposition, reduction of backgrounds, and beam diagnostics. Conventional multi-stage systems based on scatterers and absorbers offer robust shielding and efficient collection of losses. Two complementary concepts have been proposed to address some of the limitations of conventional systems: channeling and volume reflection in bent crystals and collimation with hollow electron beams. The main focus of this paper is the hollow electron beam collimator, a novel concept based on the interaction of the circulating beam with a 5-keV, magnetically confined, pulsed hollow electron beam in a 2-m-long section of the ring. The electrons enclose the circulating beam, kicking halo particles transversely and leaving the beam core unperturbed. By acting as a tunable diffusion enhancer and not as a hard aperture limitation, the hollow electron beam collimator extends conventional collimation systems beyond the intensity limits imposed by tolerable losses. The concept was tested experimentally at the Fermilab Tevatron proton-antiproton collider. Results on the collimation of 980-GeV antiprotons are presented, together with prospects for the future.

1. Introduction

In high-power accelerators, the stored beam energy can be large: about 2 MJ in the Tevatron, and several hundred megajoules in the LHC at nominal energies and intensities. Uncontrolled losses of even a small fraction of particles can damage components, cause magnets to lose superconductivity, and increase experimental backgrounds. Contributing to these losses is the beam halo, continuously replenished by beam-gas and intrabeam scattering, ground motion, electrical noise in the accelerating cavities, resonances and, in the case of colliders, beam-beam forces.

The beam collimation system is therefore vital for the operation of high-power machines. Conventional collimation schemes include scatterers and absorbers, possibly including several stages. Primary collimators are the devices closest to the beam. They impart random transverse kicks, mainly due to multiple Coulomb scattering, to particles in the halo. The affected particles have increasing oscillation amplitudes and a large fraction of them is captured by the secondary collimators. These systems offer robust shielding of sensitive components. They are also very efficient in reducing beam losses at the experiments. As an example, a description of the Tevatron collimation system can be found in Ref. [1].

The classic multi-stage system does have limitiations: a fraction of particles is always lost around the ring (leakage); collimator jaws have an electromagnetic impedance (wakefields); and high losses are generated during collimator setup when the jaws are moved inward. Another problem is beam jitter. The orbit of the circulating beam oscillates due ground motion and other vibrations. Even with active orbit stabilization, the beam centroid can oscillate by tens of microns. This translates into periodic bursts of losses at aperture restrictions.

Bent crystals and the hollow electron beam collimator are two advanced techniques to address these limitations in complementary ways. Channeling and volume reflection in bent crystals reduce leakage by directing halo particles deeper into the absorbers in a single pass [2–6]. They replace the random kicks of multiple scattering with well-defined deflections.

In this paper, we focus on the nature of the hollow electron beam collimator and on the experiments conducted in the Tevatron collider to study whether it is a viable complement to conventional systems.

2. The hollow electron beam collimator

The hollow electron beam collimator (HEBC) is a cylindrical, hollow, magnetically confined, possibly pulsed electron beam overlapping with the beam halo [7–12] (Figure 1). Electrons enclose the circulating beam. Halo particles are kicked transversely by the electromagnetic field of the electrons. If the hollow charge distribution is axially symmetric, the core of the circulating beam does not experience any electric or magnetic fields. For typical parameters, the transverse kick given to 980-GeV protons or antiprotons is of the order of 0.2 μrad. This

*On leave from Istituto Nazionale di Fisica Nucleare (INFN), Sezione di Ferrara, Italy.

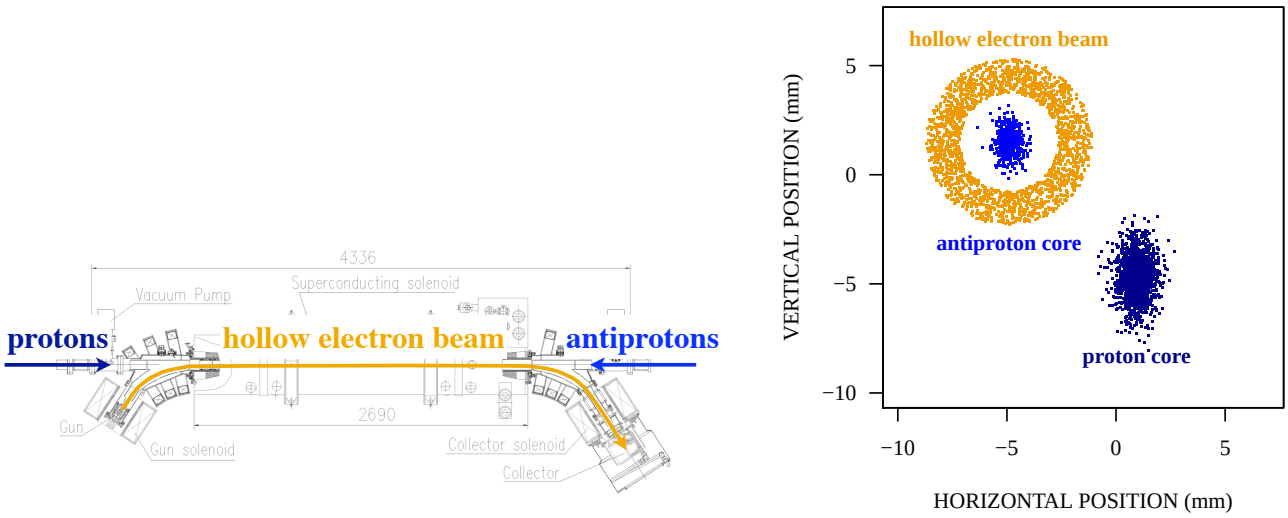

Figure 1: Hollow electron beam collimator: (left) top view; (right) schematic transverse view of the three beams.

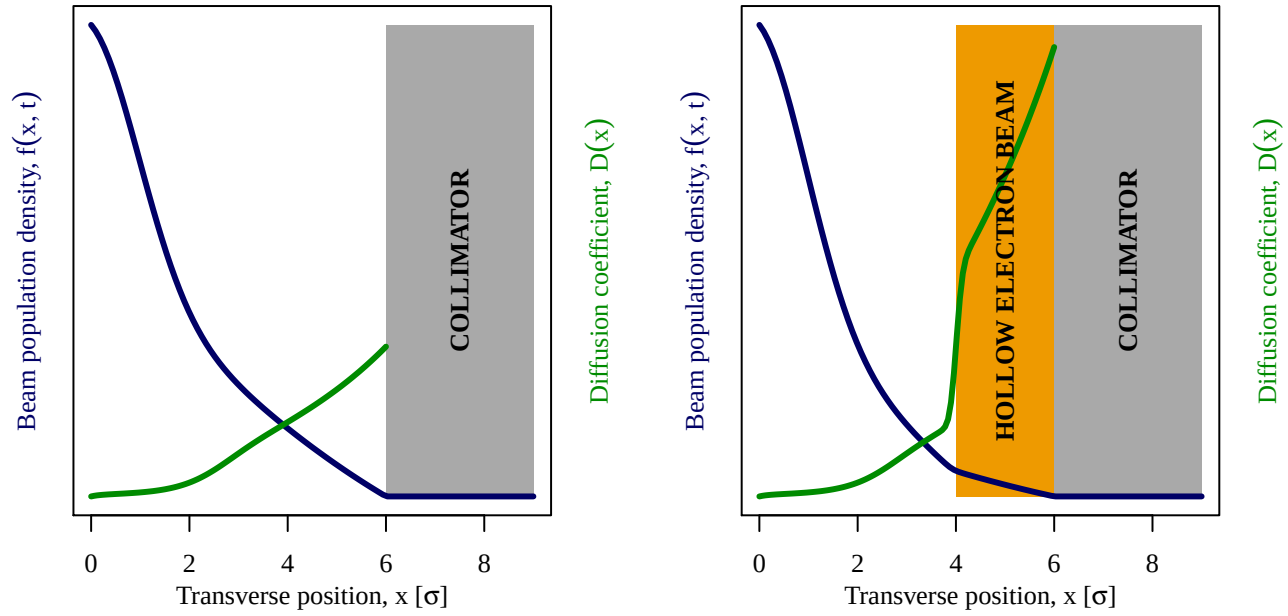

Figure 2: Schematic representation of the diffusion model of collimation with and without the hollow electron beam.

is to be compared with the multiple-scattering random kick of 17 μrad from the primary tungsten collimators in the Tevatron.

The effect of the electron lens can be understood in terms of a diffusion model of collimation (Figure 2). The beam distribution has a core with long tails (the halo). The diffusion coefficient is an increasing function of amplitude because of lattice and beam-beam nonlinearities. The collimators define the aperture of the machine, or the point where the population density is practically zero. In the diffusion model, the local loss rate is the particle flux at the collimator. It is proportional to the product of diffusion rate and density gradient. With the hollow electron lens, one aims at enhancing diffusion of the tails, reducing their population. This will decrease the loss spikes caused by collimator setup and by beam jitter.

A magnetically confined electron beam has several advantages. It can be placed very close to, and even overlap with the circulating beam. The transverse kicks are small and tunable, so that the device acts more like a “soft collimator” or a “diffusion enhancer,” rather than a hard aperture limitation. At even higher electron currents (which have not been demonstrated so far) the electron beam could become an indestructible primary collimator. If needed, the electron beam can be pulsed resonantly with the betatron oscillations to remove

particles faster. In the case of ion collimation, there is no nuclear breakup. Finally, the device relies on the estabilished technologies of electron cooling [13] and electron lenses [14–17]. One disadvantage may be the cost and complexity of the required components, such as superconducting solenoids, magnet and high-voltage power supplies, and cryogenics.

3. Beam experiments at the Tevatron

The concept of hollow electron beam collimation was tested experimentally in the Fermilab Tevatron collider (Figure 3). In the Tevatron, 36 proton bunches collided with 36 antiproton bunches at an energy of 980 GeV per beam. Each particle species was arranged in 3 trains of 12 bunches each. Initial beam intensities were typically 3×10^{11} protons/bunch and 10^{11} antiprotons/bunch. Beam lifetimes ranged between 10 h and 100 h. There were 2 head-on interaction points, corresponding to the CDF and the DZero experiments. The maximum luminosity was 4×10^{32} cm^{-2} s^{-1}. The machine operated with betatron tunes near 20.58.

A 15-mm-diameter hollow electron gun was designed and built (Figure 4). It was based on a tungsten dispenser cathode with a 9-mm-diameter hole bored through the axis of its convex surface. The peak current delivered by this gun was 1.1 A at 5 kV. The current density profile was measured on a test stand by recording the current through a pinhole in the collector while changing the position of the beam in small steps. A sample measurement is shown in Figure 4. In August 2010, the gun was installed in one of the Tevatron electron lenses (TEL2), located in the A sector of the ring. Experiments were done with antiprotons because of their smaller size and because of the configuration of the Tevatron collimation system. For antiprotons, tungsten primaries (F49 in Figure 3) were located downstream of the electron lens. Stainless-steel secondaries were placed at the F48 and D17 locations in the ring.

In the electron lens, protons and antiprotons were separated transversely and in time. The transverse separation was about 6 mm both horizontally and vertically (Figure 1). The radius of the hole was controlled by the ratio of solenoid fields. Three corrector coils were used to align the electron beam with the circulating beam. Thanks to the special high-voltage modulator, the electron beam could be synchronized practically with any group of bunches. In the oscilloscope picture of Figure 5, one can see the short proton and antiproton bunches in cyan, and the shortest possible electron pulse in magenta. Alignment of the beams was found to be reliable and reproducible. The stability of the system of three beams was not an issue at solenoid fields above 10 kG.

Experiments in the Tevatron started in October 2010 and ended with the shutdown of the machine in September 2011. Many observables such as particle removal rates, effects on the core, diffusion enhancement, collimation

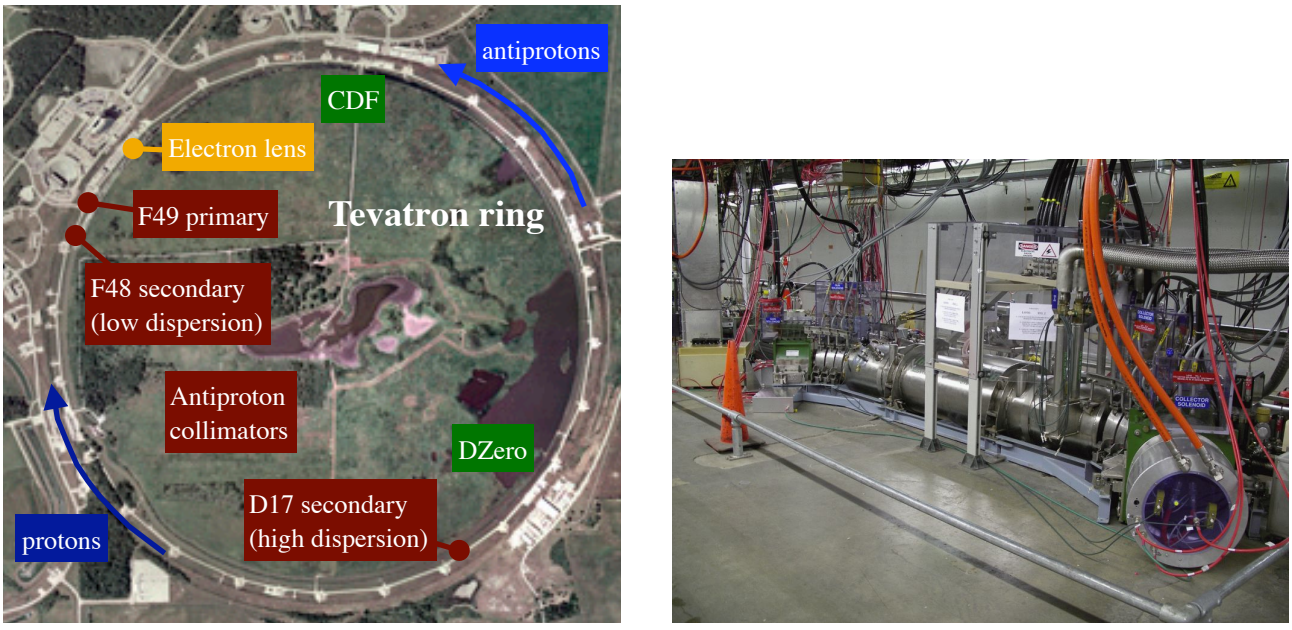

Figure 3: (left) Layout of the hollow-beam collimation experiments. (right) Photograph taken in the Tevatron tunnel of the electron lens (TEL2) used as hollow-beam collimator.

efficiency and loss rate fluctuations were measured as a function of electron lens parameters: beam current, relative alignment, hole radius, pulsing pattern, and collimator configuration. Preliminary results were presented in Refs. [18–20]. Here, a few examples of the main effects are shown.

3.1. Particle removal rates

The first question we addressed was the particle removal rate. Can these small transverse kicks have a detectable effect? The experiment in Figure 6 (left) shows the scraping effect. The electron lens was aligned and synchronized with the second antiproton bunch train, and then turned on and off several times at the end of a collider store. The electron beam current was about 0.4 A and the radius of the hole was varied between 6 and 3.5 standard deviations (σ) of the vertical beam size. The black trace is the electron-lens current. To isolate the effect of the hollow beam, Figure 6 (left) shows the ratio between the intensity of the affected train and the average intensity of the other two control trains. One can clearly see the smooth scraping effect. The

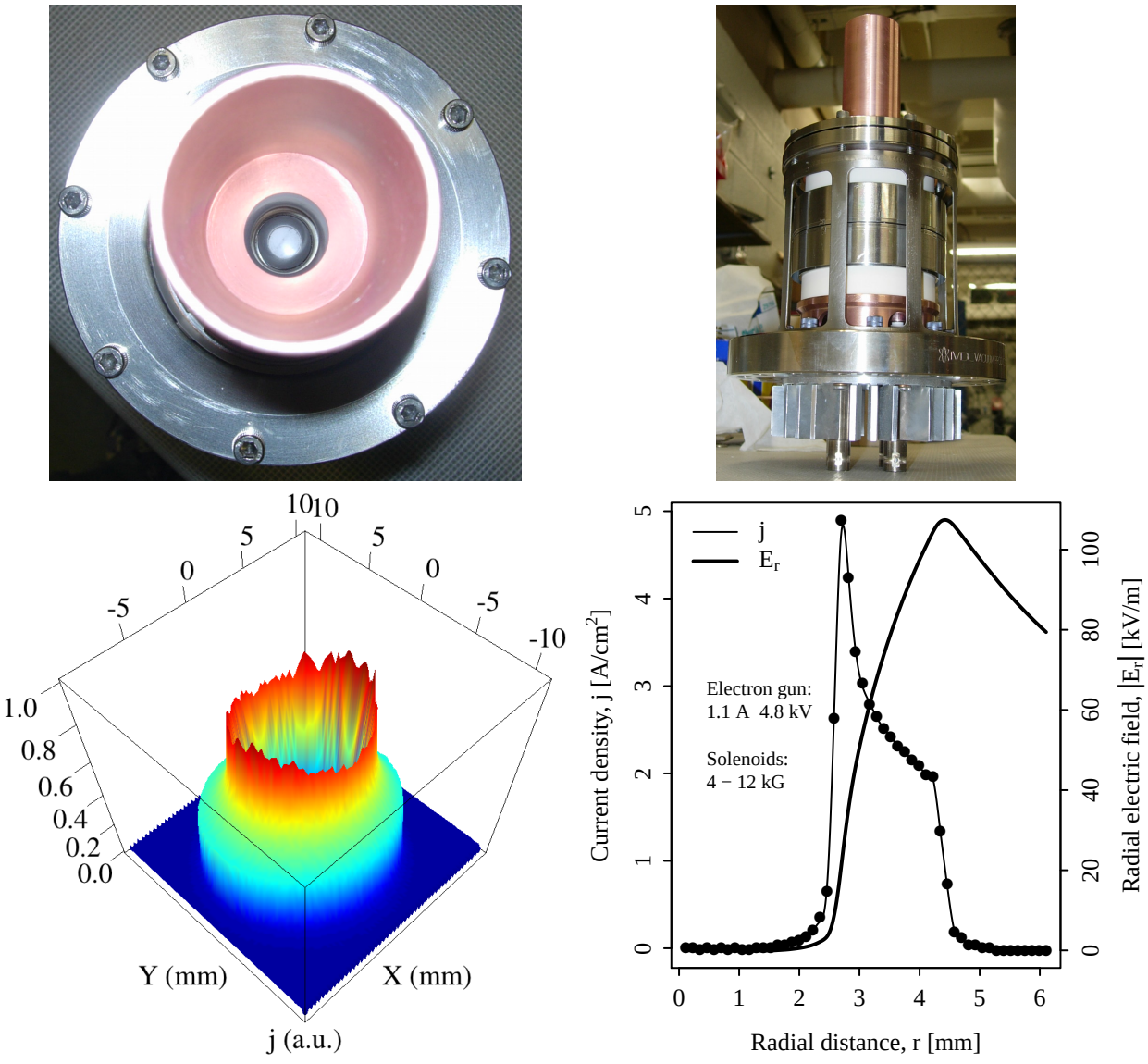

Figure 4: 15-mm hollow electron gun used in the Tevatron experiments: (top left) photograph of the copper anode and of the hollow tungsten cathode; (top right) photograph of the assembled gun; (bottom left) example of measured transverse current profile; (bottom right) example of radial current density distribution and electric field in the overlap region for a total current of 1.1 A and a magnetic compression factor of $\sqrt{(4\text{ kG})/(12\text{ kG})} = 0.58$.

corresponding removal rates are a few percent per hour, and increase with decreasing hole radii. One can also see that there were no adverse effects with large hole sizes. This allowed us to do many experiments parasitically during regular collider stores.

3.2. Effects on the beam core

Which particles are being removed? Whether there are any adverse effects on the core of the circulating beam is a concern. The overlap region is not a perfect hollow cylinder, due to asymmetries in gun emission, to evolution under space charge of the hollow profile, and to the bends in the transport system.

We estimated the effects on the core from several points of view: particle removal rates, emittance growth, luminosity, and diffusion enhancement vs. amplitude. First, one can see from Figure 6 (left) that no decrease in intensity was observed with large hole sizes, when the hollow beam was shadowed by the primary collimators. This implies that the circulating beam was not significantly affected by the hollow electron beam surrounding it, and that the effect on beam intensity of residual fields near the axis was negligible.

Secondly, one can observe the evolution of the emittances. In Figure 6 (right), the average emittances of the affected bunch train are shown. If there was emittance growth produced by the electron beam, it was much smaller than that driven by the other two main factors, intrabeam scattering and beam-beam interactions. As expected, for small hole sizes, suppression of the beam tails translated into a reduction in measured transverse emittances.

The effect of halo removal can also be observed by comparing beam scraping with the corresponding decrease in luminosity. Luminosity is proportional to the product of antiproton and proton populations, and inversely proportional to the overlap area. If antiprotons were removed uniformly and the other factors were left unchanged, luminosity would decrease by the same relative amount. If the hollow beam caused emittance growth or proton loss, luminosity would decrease even more. Because of the smaller relative contribution to luminosity of halo particles, a smaller relative change in luminosity is a clear indication of halo scraping. In Figure 6 (left), one can see how the luminosity for the affected bunch train changed with time relative to the average

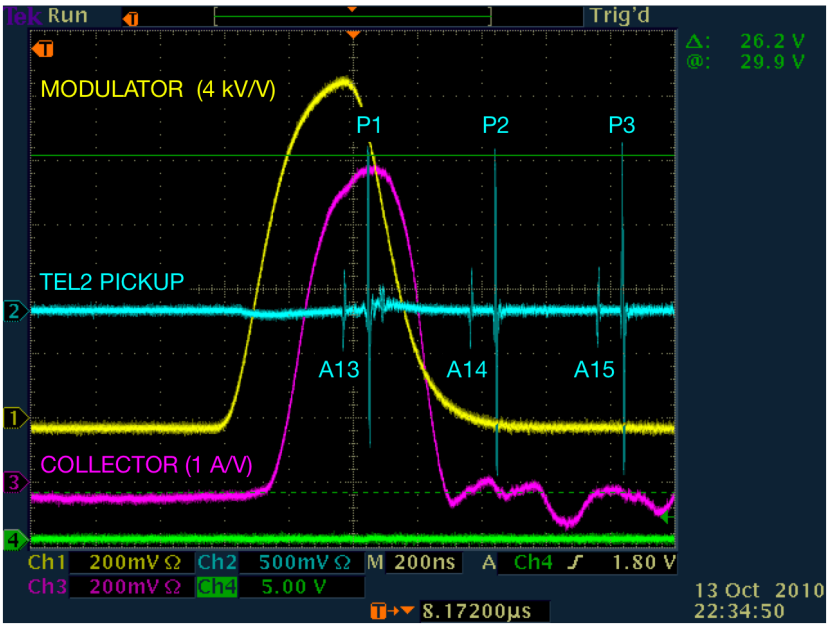

Figure 5: Synchronization of the electron beam pulse with an antiproton bunch: modulator voltage (yellow); electron current in the collector (magenta); pickup signal (cyan) showing three proton bunches (P1–P3), three antiproton bunches (A13–A15), and the derivative of the electron pulse.

luminosity of the control bunch trains. The dark cyan trace is the ratio between affected and control trains. The corresponding relative luminosity decay rates are smaller that those of intensity. As expected, luminosity decay rates approach intensity decay rates as the radius of the hole is decreased.

3.3. Diffusion enhancement

It is possible to measure transverse beam diffusion rates as a function of betatron amplitude by observing the time evolution of losses as collimators are moved in small steps [21–24] (Figure 7, top left). The main features of the response of local losses to small inward collimator steps are a sharp peak and a decay proportional to the inverse square root of time. From this decay the diffusion rate at the location of the collimator can be extracted. Figure 7 (top right) shows an example of a collimator scan. The vertical F48 secondary collimator was moved in 50-μm steps towards the beam center. All other collimators were retracted. The characteristic decay time is a function of collimator position. These loss spikes are what constrained the tightest collimator settings and limited their setup. Even when the collimators were moved in micron-size steps, below about 4σ in transverse beam size these spikes could exceed the quench limits in the Tevatron superconducting magnets. Figure 7 (bottom left) shows an example of diffusion measurements vs. amplitude at the end of a regular collider store. Similar to the results obtained in the HERA machine at DESY [21, 22], a strong dependence of the diffusion coefficient with amplitude is observed. More details can be found in Refs. [23, 24].

We are interested in how the hollow beam affects diffusion. New scintillator paddles were installed near one of the antiproton secondary collimators during a short shutdown in March 2011. These loss monitors were gated to individual bunch trains. With this device we could measure diffusion rates, collimation efficiencies and loss spikes simultaneously for the affected and the control bunch trains. An example of what can be observed by comparing losses from different bunches is shown in Figure 7 (bottom right). The electron lens was aligned and synchronized with bunch train #2 with a peak current of 0.9 A. The plot shows the response of local losses to an outward collimator step. In this case, one observes a dip instead of a spike. The difference in diffusion times between the control and the affected train is apparent. It corresponds to an enhancement of the diffusion rate by a factor 10. Because the steady-state loss rate is the product of diffusion coefficient and gradient of the beam population, the fact that it is only 10% higher for the affected train indicates that the halo population was reduced by approximately a factor 10 as well.

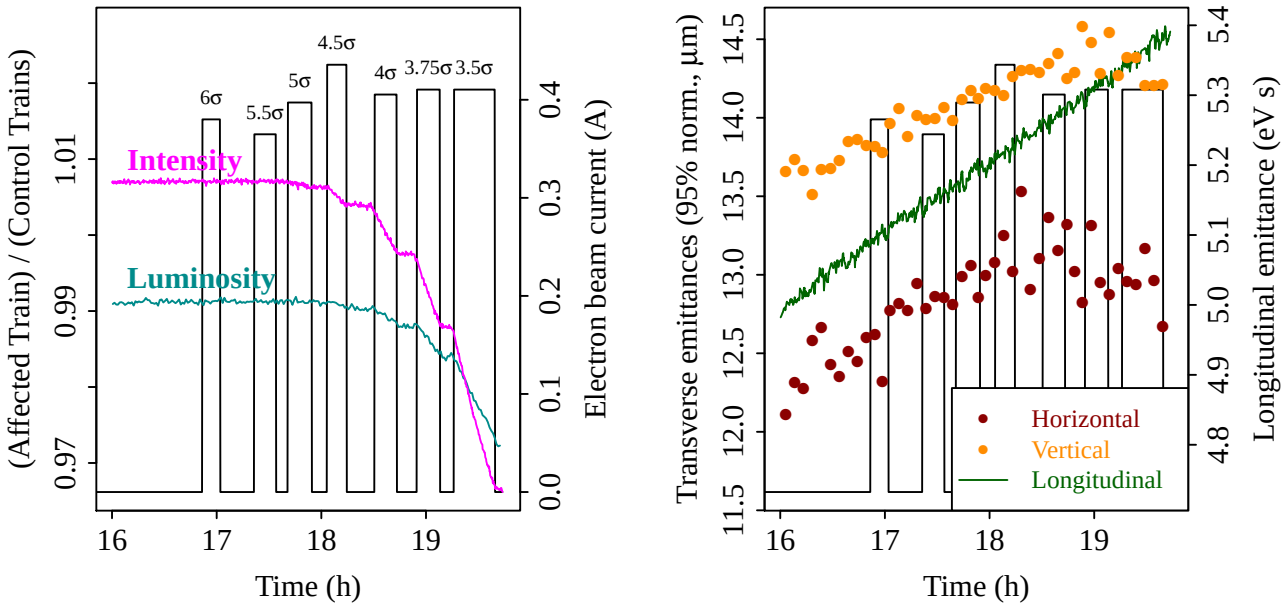

Figure 6: Effects of the hollow electron beam collimator on 980-GeV antiprotons in the Tevatron at the end of a regular collider store, for different values of the hole radius. (left) Relative intensity and luminosity of the affected bunch train; (right) transverse and longitudinal emittances of the affected bunch train during the same experiment. The black trace represents the intensity of the electron beam.

3.4. Mitigation of beam jitter

In Figure 7 (bottom right), one may notice some of the periodic losses due to beam jitter in the control train. They are suppressed in the affected train: another indication of halo removal. This effect is also apparent in the Fourier spectrum of gated losses (Figure 8, left). Normally, the spectra showed peaks corresponding to mechanical vibrations caused, for instance, by the Main Injector acceleration ramp (0.3 Hz) or by the compressors of the Central Helium Liquefier (4.6 Hz). The electron beam acting on the second bunch train suppressed these periodic losses. This is another manifestation of the reduction of tails.

A better understanding of the distribution of these losses comes from the analysis of their correlations. The

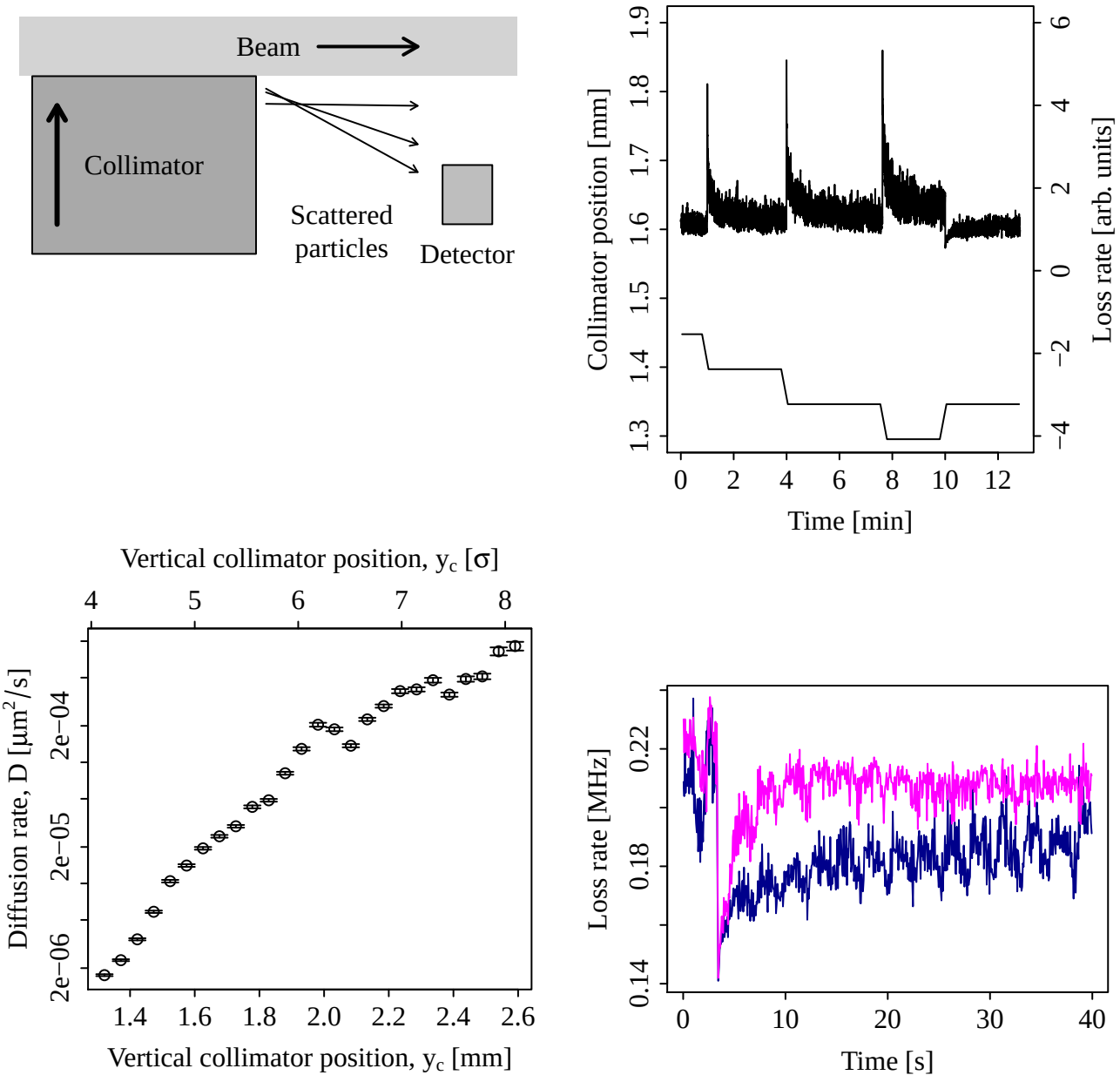

Figure 7: Measurements of transverse beam diffusion with collimator scans. (top left) Schematic view of the experiment: local losses are measured as a collimator is moved inward or outward in small steps. (top right) Example of measured loss rates as the F48 secondary antiproton collimator is moved inward (3 steps) and outward (1 step) by 50 μm. (bottom left) Measurement of diffusion rate vs. amplitude with a collimator scan in the Tevatron. (bottom right) Simultaneous measurement of local loss rates in response to an outward step for the control bunch train (blue) and the bunch train affected by the hollow electron beam (magenta), demonstrating diffusion enhancement.

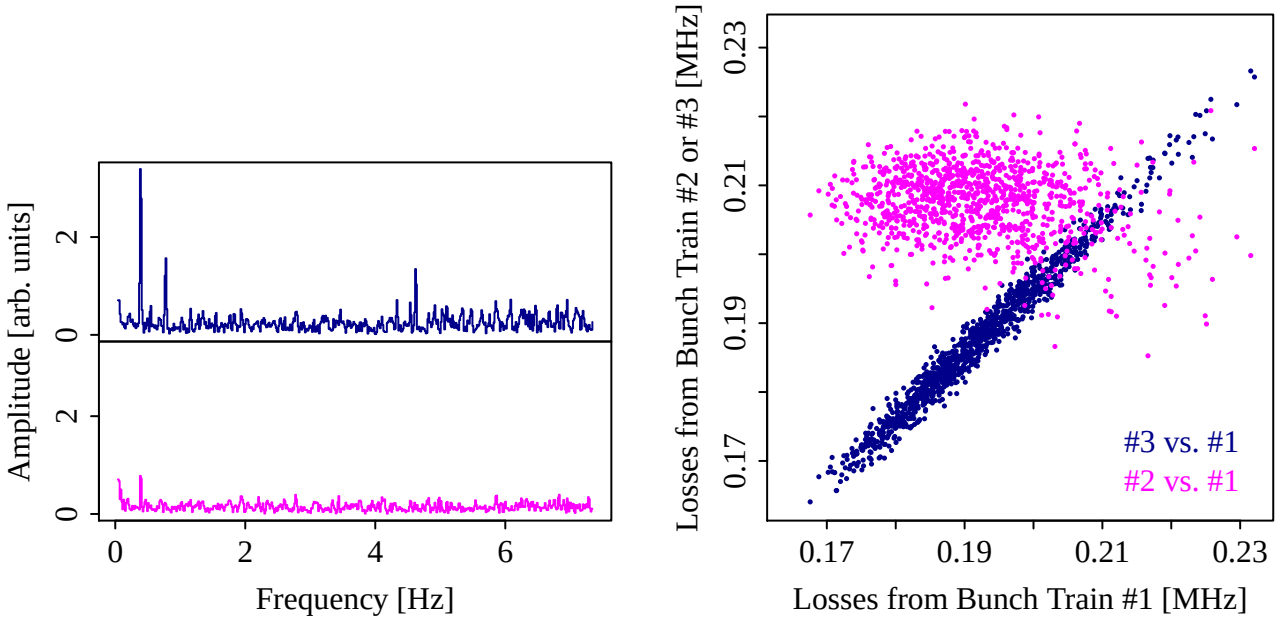

Figure 8: Simultaneous measurement of steady-state loss rates for the two control bunch trains (#1 and #3) and for the bunch train affected by the hollow electron beam (#2). (left) Frequency spectrum of losses: control train #1 (blue) and affected train #2 (magenta); coherent peaks due to vibrations are suppressed. (right) Correlation between loss rates: #3 vs. #1 (blue), showing that beam jitter dominates loss fluctuations; #2 vs. #1 (magenta) shows that correlation is removed and peaks due to beam jitter are mitigated.

blue points in Figure 8 (right) show the losses coming from train #3 vs. those from train #1. These are the two control bunches. One can see random fluctuations of the order of 2 kHz out of 0.2 MHz. But the main effect is a very high correlation. Most of the fluctuations are not random, but coherent. They can be attributed to beam jitter. The effect of the hollow beam is to eliminate this correlation: average losses are increased, instantaneous losses are randomized, and the spikes are reduced. This effect can be interpreted as an increase in diffusion and a decrease in tail population, which translates into a reduced sensitivity to beam jitter.

4. Conclusions and outlook

Thanks to the dedication of all the people involved in the project, the hollow electron beam collimator now appears to be a viable tool for high-power circular accelerators. Many experimental observations of the scraping effects were made at the Tevatron using the existing electron lenses equipped with a hollow electron gun designed for this purpose.

A new 25-mm gun was designed and built. It will be tested at the Fermilab electron-lens test stand to investigate the technical feasibility of larger currents (about 3 A at 5 kV) and beam radii. We also plan to increase our effort in simulations to understand hollow-beam collimation in the Tevatron and extend it to other machines.

Some of the electron lens hardware will become available after the Tevatron shutdown. Recently, both the DOE LARP Review Committee [25] and the LHC Collimation Review Committee [26] recommended continuing the experimental program at CERN in the SPS or in the LHC. In collaboration with the LHC Collimation Working Group, we are studying whether a hollow-beam scraper is applicable to the CERN machines.

Acknowledgments

The work on hollow electron beam collimation was done in collaboration with A. Valishev, J. Annala, T. Johnson, G. Saewert, V. Shiltsev, D. Still, and L. Vorobiev of Fermilab.

This project would not have been possible without the support of the Fermilab Accelerator Division and of the CDF and DZero collaborations. In particular, I would like to thank M. Convery, C. Gattuso, and R. Moore

for their invaluable support. Fermi Research Alliance, LLC operates Fermilab under Contract No. DE-AC02-07CH11359 with the US Department of Energy. This work was partially supported by the US LHC Accelerator Research Program (LARP).

References

1 N. Mokhov et al., JINST **6**, T08005 (2011), Report No. FERMILAB-PUB-11-378-APC.
2 E. N. Tsyganov, Report No. FERMILAB-TM-0682 (1976).
3 M. A. Maslov, N. V. Mokhov, and I. A. Yazynin, Report No. SSCL-484 (1991).
4 W. Scandale et al., Phys. Rev. Lett. **102**, 084801 (2009).
5 V. Zvoda et al., in *Proc. 2011 Part. Accel. Conf. (PAC11)*, New York, NY, Report No. FERMILAB-CONF-11-127-APC.
6 W. Scandale, in *Proc. 2nd Int. Part. Accel. Conf. (IPAC11)*, San Sebastián, Spain, Paper ID TUOAA02 (2011).
7 V. Shiltsev, in *Proc. 3rd CARE-HHH-APD Workshop (LHC-LUMI-06)*, Valencia, Spain, p. 92, Report No. CERN-2007-002 (2007).
8 V. Shiltsev, in *Proc. CARE-HHH-APD Workshop (BEAM07)*, Geneva, Switzerland, p. 46, Report No. CERN-2008-005 (2007).
9 V. Shiltsev et al., in *Proc. 2008 Eur. Part. Accel. Conf. (EPAC08)*, Genoa, Italy, p. 292, Report No. FERMILAB-CONF-08-184-APC (2008).
10 J. C. Smith et al., in *Proc. 2009 Part. Accel. Conf. (PAC09)*, Vancouver, Canada, p. 2856, Report No. FERMILAB-CONF-09-412-APC (2009).
11 G. Stancari et al., in *Proc. 1st Int. Part. Accel. Conf. (IPAC10)*, Kyoto, Japan, p. 1698, Report No. FERMILAB-CONF-10-182-AD-APC (2010).
12 G. Stancari et al., Proc. 14th Adv. Accel. Concepts Workshop (AAC10), AIP Conf. Proc. **1299**, 638 (2010), Report No. FERMILAB-CONF-10-196-APC (2010).
13 V. V. Parkhomchuk and A. N. Skrinsky, Rev. Accel. Sci. Tech. **1**, 237 (2008).
14 V. Shiltsev et al., Phys. Rev. Lett. **99**, 244801 (2007).
15 V. Shiltsev et al., New J. Phys. **10**, 043042 (2008).
16 V. Shiltsev et al., Phys. Rev. ST Accel. Beams **11**, 103501 (2008).
17 X.-L. Zhang et al., Phys. Rev. ST Accel. Beams **11**, 051002 (2008).
18 G. Stancari et al., in *Proc. 2011 Part. Accel. Conf. (PAC11)*, New York, NY, Paper ID MOP147, Report No. FERMILAB-CONF-11-058-AD-APC (2011).
19 G. Stancari et al., Phys. Rev. Lett. **107**, 084802 (2011), Report No. FERMILAB-PUB-11-192-AD-APC (2011).
20 G. Stancari et al., in *Proc. 2nd Int. Part. Accel. Conf. (IPAC11)*, San Sebastián, Spain, Paper ID WEODA02, Report No. FERMILAB-CONF-11-412-AD-APC (2011).
21 K.-H. Mess and M. Seidel, Nucl. Instrum. Methods Phys. Res. A **351**, 279 (1994).
22 M. Seidel, Ph.D. Thesis, Hamburg University, Report No. DESY-94-103 (1994).
23 G. Stancari, arXiv:1108.5010, Report No. FERMILAB-FN-0926-APC (2011).
24 G. Stancari et al., in *Proc. 2nd Int. Part. Accel. Conf. (IPAC11)*, San Sebastián, Spain, Paper ID TUPZ033, Report No. FERMILAB-CONF-11-411-AD-APC (2011).
25 US DOE LARP Review Report, Fermilab, June 2011, `<https://indico.fnal.gov/event/4380>` (unpublished).
26 LHC Collimation Review Report, CERN, June 2011, `<http://indico.cern.ch/event/collreview2011>` (unpublished).